Method for extracting an equivalent Winkler model of the 3D dynamic soil-structure interaction of large-diameter offshore monopile foundations

W.G. Versteijlen J.M. de Oliveira Barbosa K.N. van Dalen A.V. Metrikine
pim.versteijlen@siemens.com

Abstract

The motivation for this work stems from the offshore wind industry, where designers are faced with a discrepancy between the available design methods and the typical dimensions of the offshore wind foundations that call for other design approaches. Throughout the years, much valuable work has been performed in the prediction of long, slender, flexible piles which are most often applied in the field. For the large-diameter rigidly behaving 'caisson' foundations, less methods are available. These two types of piles (flexible and rigid) interact in a fundamentally different way with the soil. The fact that the observed fundamental frequencies of installed offshore wind structures are higher than designed for, is believed to confirm the underestimation of stiffness associated with the often used 'p-y' design method.

For the damping related part, being it a more complex mechanism, there is even more uncertainty. As a result, conservative low damping ratios are assumed during design. Though it is less straightforward to measure the damping ratios of installed turbines, the published values range from a factor of 1 to 4 with respect to the value used in design. Like for stiffness, empirical relations were derived to estimate damping in the 1970s and 80s based on more advanced 2D and 3D models in combination with field tests and the previously mentioned p-y curves. Again, these relations are restricted to flexible piles, where the pile tip is assumed to be fixed.

To capture the interaction for the currently applied pile dimensions, it is necessary to simulate the 3D interaction between the pile and the soil, and perform full scale tests. The latter are not yet available, but results of a few campaigns are expected in the near future. Advanced 3D numerical models are available, and for the purpose of physical insight and for engineering applications, it is useful to extract a 1D equivalent model that can mimic the 3D simulation.

In this work, a linear elastic dynamic 3D FE model of a pile-soil system is used to extract the static and the frequency dependent displacements. The FE domain is surrounded with perfectly matched layers (PMLs) that absorb the propagating waves at the boundaries for the relevant frequencies of excitation. The soil properties of a design location are used, which have been

identified using seismic measurements. A method for the derivation of a 1D equivalent dynamic stiffness (i.e., a Winkler model with distributed springs and dashpots) is derived thereafter. The results obtained with the 1D model for the static response and for a dynamic case are compared to the response of the 3D FE analysis.

1 Introduction

The fundamentally different behaviour between long, slender piles and those with a small ratio of embedded length L over diameter D is widely recognized. Many parametric studies have indicated that this L/D ratio, together with the ratio of the pile stiffness over the soil stiffness is what determines the characteristic response. Pile flexibility factors [1] and characteristic lengths [2] can be calculated to predict the typical response (whether rigid or flexible behaviour is to be expected). In general, piles with a small L/D ratio ($L/D < 7$ for most soil-steel stiffness combinations) bend in a rigid way, interacting on a more global scale with the soil, whereas the displacement and moment distribution of flexible piles can be attributed to local soil reactions. The motivation for the here presented work stems from the offshore wind industry, where rigid behaving foundations (with $4 < L/D < 7$) are designed based on design methods that were developed for flexible long piles with $L/D \approx 30$. In general it holds that many more thoroughly tested methods have been developed for flexible piles (the most often applied type of pile) than for rigid behaving piles. Not much full-scale testing has so far been performed on rigid behaving piles; however, current numerical (Finite Element Methods (FEM)) competences are more and more capable of capturing the complex 3D nature that characterizes the global soil reaction [8]. This is not only the case for the static reaction; due to successful mitigation of reflections at the boundaries, also dynamic analyses can be performed with higher levels of confidence. Also complicated poro-elastic mechanisms (contributing to both the stiffness and damping characteristics of the soil-structure interaction (SSI)) have been modeled in 3D numerical models [3]. However, as previously mentioned the full-scale testing database needs to become available to fully validate the developed models.

The 3D models are well fit to capture a more realistic response for a certain load case. Nevertheless, their high computational cost makes them incompatible with engineering design. For instance, in the offshore wind industry up to 10.000 simulations of 10min-time responses are run for a single design location and iteration. Despite efficient upcoming numerical substructering techniques [4], it is for many designers not yet feasible to incorporate full 3D numerical models in these kind of design simulations. This is one of the reasons that a more simple and fast equivalent 'engineering' model is desired. The second reason would be the fact that due to the simplification, often more physical insight is gained in capturing the complex 3D nature in a 1D model. In this work, we choose to match the response with a 1D model (and not for instance, a lumped parameter model with discrete springs at the mudline) as this allows to assess the stress distribution in the embedded pile, which is also often assessed in design. Besides these advantages, the coupling terms

between the translation and rotation are automatically incorporated.

Before we can build a 3D model, we need to find the continuum (soil) input parameters. This is shortly discussed in Section 2, where we advocate the use of seismic measurements (besides the usual geotechnical in-situ testing) to capture the dynamic properties of the soil. Section 3 gives a brief description of the linear elastic 3D model that incorporates material and radiation damping, and efficiently deals with the reflective boundary problem. Then, being the emphasis of this contribution, the translation method of both the static and the complex (dynamic) 3D modeled response into an equivalent 1D model is given in Section 4. Then, Section 5 closes the paper with a discussion on the presented results.

2 Soil characterization

In this paper we focus on the linear reaction regime of the soil, as it is this regime that defines the modal response of the support structure. To extract the linear elastic properties of a certain site, we suggest to perform in-situ seismic measurements along with the usual geotechnical testing procedures (i.e. Cone Penetration Tests (CPT) and laboratory test on borehole samples). The latter are useful for (local) strength parameters, stratification and density estimation, whereas the seismic measurements capture the true dynamic, small-strain characteristics of the soil.

We emphasize the advantage of *in-situ* seismic measurements because of two reasons: firstly, the in-situ characteristics are always disturbed when retrieving soil samples. Secondly, depending on the frequency of interest, it might be challenging to test soil samples in a laboratory without including sample-boundary effects. It is favorable to be able to capture at least one wave length within a sample, but for the low frequencies (< 1 Hz), shear-wave lengths are typically in the order of several hundreds of meters ($\lambda = \frac{V_s}{f}$, with λ the shear wave length, V_s the shear wave velocity and f the frequency of interest).

Multiple seismic measurement set-ups exist, among which are Multi-Channel Analyses of Surface Waves (MASW), P&S logging, cross/down/up-hole measurements and the Seismic Cone Penetration Test (SCPT). All these tests have their own inversion techniques. In [5] an inversion method for SCPT data is given.

For this paper, we use a soil profile which was identified using SCPT data (to be published in the near-future). The elastic parameters of this profile are given in Figure 1.

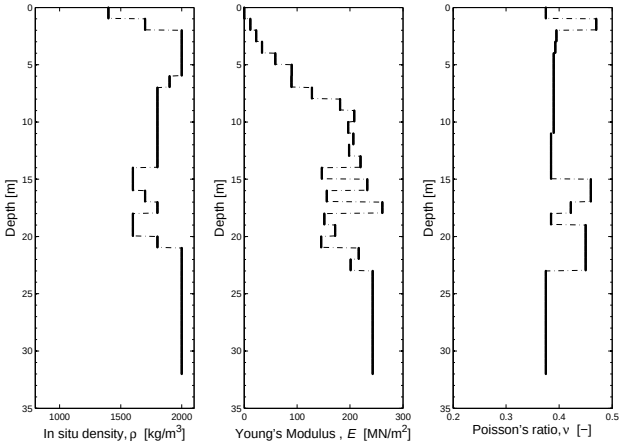

Figure 1: Profiles of the elastic parameters used in the 3D model; density ρ (left panel), Young's modulus E (middle panel) and Poisson's ratio ν (right panel).

With these elastic continuum parameters (Young's modulus E, density ρ and Poisson's ratio ν) at hand, we are ready to construct a 3D elastic model.

3 3D model

For the large diameter rigidly behaving foundations, we need to incorporate 3D effects; the interaction between soil and the large foundation mobilizes more global reactions of the soil instead of local (as is the case for slender piles). This more rigorous model consists of a 2D axisymmetric domain, in which both the soil as the pile are modeled with solid finite elements [6]. To avoid reflections at the edges of the domain, Perfectly Matched Layers (PMLs) (as defined in [7]) are added to the outer boundary of the domain. For very low frequencies, the PMLs are replaced by elastic layers whose dimensions are large enough so that the fictitious boundaries do not influence the results. In order to keep the calculation times small, the size of the elements composing these buffer layers are made successively larger as the distance to the pile increases. The loading scenario of interest is a horizontal load F at the free end of the pile and a bending moment m at the same end. In the more realistic scenario, these loads can be expressed in terms of radial F_R, tangential F_T and vertical F_V forces as

$$F = R \int_0^{2\pi} \left(F_R(\theta) \cos\theta - F_T(\theta) \sin\theta \right) \mathrm{d}\theta, \tag{1}$$

$$m = R^2 \int_0^{2\pi} F_V(\theta) \cos\theta \, \mathrm{d}\theta, \tag{2}$$

where θ is the angle with respect to the horizontal direction of the load F, and R is the radius of the pile. Assuming that the horizontal force F is equally distributed

along the perimeter of the pile, then the radial and tangential forces are of the form

$$F_R(\theta) = \frac{F_H}{2\pi R}\cos\theta, \tag{3}$$

$$F_T(\theta) = \frac{F_H}{2\pi R}\sin\theta. \tag{4}$$

Likewise, the force F_V can be described with the cosine of θ as

$$F_V(\theta) = \frac{m}{\pi R^2}\cos\theta. \tag{5}$$

The Fourier expansion of F_R, F_T and F_V leaves us only with terms of first order, and therefore the axisymmetric problem needs to be solved only for the first Fourier term, as explained in reference [6]. Solving this axisymmetric problem is computationally more efficient than solving a complete 3D problem (much smaller linear systems) and produces as accurate results (if not better), provided that the true force distributions along the free end of the pile are as assumed.

For this example, the material damping for both pressure as shear waves was set equal to a ratio of 1%. The soil profile as given in Figure 1 was used. The embedded pile length was set on 32m and its diameter and wall-thickness on 5m and 6cm respectively, giving an L/D ratio of 6.4, which can be considered a rather rigid pile in typical soil conditions. Of course, also typical steel properties were given to the pile; a density of $7850\,kg/m^3$, a Young's modulus of $2.1\times10^{11}N/m^2$ and a Poisson's ratio of 0.3. The vertical model boundary (horizontal plane) was set at 50m depth. Figures 2 and 3 give a qualitative impression of the 3D pile deflection, and soil-stress response respectively.

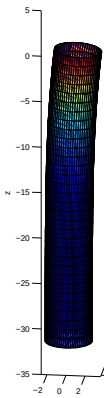

Figure 2: 3D pile deflection due to lateral force

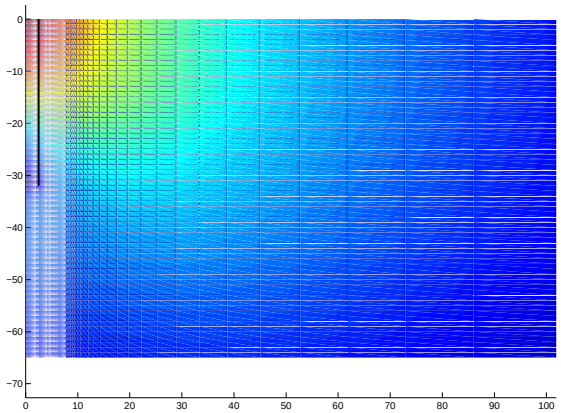

Figure 3: A qualitative impression of soil-stresses in the 3D model

4 An equivalent 1D model

In this paper, the method for finding an equivalent beam on Winkler foundation is demonstrated for the case that only a unit horizontal force of 1N is applied at the

top of the pile with a frequency of 0.2 Hz. As the level of the top of the pile in the 3D model is 1cm above mudline, a small bending moment is also applied at mudline. We will only use the averaged 3D horizontal displacement (the centerline of the pile, which is found by averaging the nodes of the cross-sections). This displacement and its derivatives are used within the Euler-Bernoulli formulations for a beam. Though the resistance mechanisms of the soil are quite complex in reality, we will, like often done in engineering models, limit ourselves to only considering distributed lateral springs. To ensure an equilibrium of forces at the boundaries, we do allow discrete lateral and rotational springs at these locations.

First, a static reaction is calculated in the 3D model, in order to find the static soil stiffness $k_s(z)$. Afterwards, a forcing at a frequency of 0.2 Hz is applied. It is then attempted to match both the real as the imaginary part of the resulting 3D deflection in the 1D model by finding an equivalent dashpot distribution $c(z)$, assuming that the stiffness in this case can still be adequately described by the previously found static stiffness $k_s(z)$. Again, we only consider lateral dashpots, including complex discrete lateral and rotational springs at the boundaries. A schematic view of the 1D model is given in figure 4.

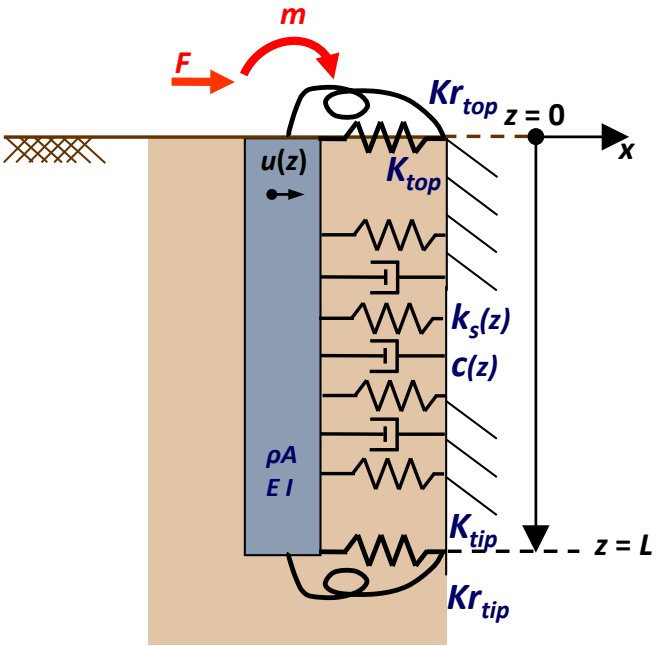

Figure 4: Schematic view of the equivalent 1D model

The material damping in the 3D model was set to a ratio of 1%, by making the Young's modulus of the soil complex. It was implemented as a hysteretic (frequency independent) damping, so also the damping term in the equation of motion (EOM) that will be considered for the beam will be of the hysteretic type. The EOM, considered in the frequency domain, thus reads

$$EI\frac{\partial^4 u(z)}{\partial z^4} + (k_s(z) + ic(z) - \omega^2 \rho A)u(z) = 0, \tag{6}$$

in which $u(z)$ is the complex amplitude of the displacement in the frequency domain, $c(z)$ the depth dependent hysteretic dashpot value, i the imaginary number ($\sqrt{-1}$), ω the angular frequency of the applied load, E the Young's modulus of the steel of the pile, ρ the material density of the steel of the pile and A and I respectively the area and the second moment of area of the cross section of the pile.

The following boundary conditions (BCs) apply:

$$EI\frac{\partial^3 u}{\partial z^3}\bigg|_{z=0} = F - K^*_{top}u(0), \tag{7}$$

$$EI\frac{\partial^2 u}{\partial z^2}\bigg|_{z=0} = m + Kr^*_{top}\frac{\partial u}{\partial z}\bigg|_{z=0}, \tag{8}$$

$$EI\frac{\partial^3 u}{\partial z^3}\bigg|_{z=L} = K^*_{tip}u(L), \tag{9}$$

$$EI\frac{\partial^2 u}{\partial z^2}\bigg|_{z=L} = -Kr^*_{tip}\frac{\partial u}{\partial z}\bigg|_{z=L}, \tag{10}$$

in which the '*' in K^*_{top}, etc. indicates that these discrete lateral and rotational springs are complex-valued dynamic stiffnesses. The magnitude of these springs can be calculated directly using the values of the 3D complex $u(z)$ and its derivatives at these locations. This ensures that the force and moment equilibria at the boundaries are satisfied according to the Euler-Bernoulli beam theory. The magnitude of the distributed springs and dashpots cannot be directly computed due to the fact that $u(z)$ often (for many soil-pile-forcing combinations) has a zero-crossing at a certain depth, which will result in singular values and negative stiffness. We thus try to find an equivalent $k_s(z)$ and $c(z)$ by taking integrals of the EOM over certain parts of the pile. As mentioned previously, first the static distributed stiffness is found by considering the static displacement of the 3D model. Afterwards, it is assumed that this $k_s(z)$ still applies for the dynamic reaction of the soil. Here, we will describe the method for finding $c(z)$, but $k_s(z)$ is found in the same way, (the inertia and damping terms are set equal to zero, and the spring constants of the discrete springs in the BCs are real). Note that for the dynamic case only $k_s(z)$ is used from the static calculation; the discrete springs are recalculated based on the complex deflections (equations 7 to 10). Then, in looking for the magnitude of $c(z)$, we assume a 'free' polynomial form:

$$c(z) = p_0 + p_1 z + p_2 z^2 + p_3 z^3 + p_4 z^4. \tag{11}$$

This expression has 5 unknowns, so we preferably need 5 equations to find these constants. As indicated, we use integrals of the EOM; 2 global integrals (from pile top (z=0) to pile tip ($z = L$)), and 3 local integrals with variable, yet unknown integration bounds. When taking the integral of the EOM (equation 6) over the full length of the pile (from 0 to L) and substituting the BC's where possible, we obtain

$$\begin{aligned}\int_0^L c(z)u(z)dz &= \left\{ -EI\frac{\partial^3 u}{\partial z^3}\bigg|_L + EI\frac{\partial^3 u}{\partial z^3}\bigg|_0 - \int_0^L k_s(z)u(z)dz + \rho A\omega^2\int_0^L u(z)dz \right\}/i \\ &= \left\{ -K^*_{tip}u(L) + F - K^*_{top}u(0) - \int_0^L k_s(z)u(z)dz + \rho A\omega^2\int_0^L u(z)dz \right\}/i,\end{aligned}$$

(12)

However, when computing $c(z)$ in this way, it will become complex due to the fact that $u(z)$ and its derivatives are complex. To avoid this, only the real parts of the left hand and right hand sides of the above equation are considered;

$$\begin{aligned} &Re(\int_0^L c(z)u(z)dz) = \\ &Re(\Big\{ -K^*_{tip}u(L) + F - K^*_{top}u(0) - \int_0^L k_s(z)u(z)dz + \rho A\omega^2 \int_0^L u(z)dz \Big\}/i). \end{aligned} \tag{13}$$

This is the case for all the integrals we take, so the '*Re*' indication will be omitted here after. The second integral is equal to the first, but multiplied with z. By doing so, we consider a moment equilibrium instead of a force equilibrium as in equations 6 and 12. Integrating by parts and substituting the BC's where possible, we get

$$\begin{aligned} &\int_0^L zc(z)u(z)dz = \\ &\Big\{ -zEI\frac{\partial^3 u}{\partial z^3}\Big]_L^0 + EI\frac{\partial^2 u}{\partial z^2}\Big]_L^0 - \int_0^L zk_s(z)u(z)dz + \rho A\omega^2 \int_0^L zu(z)dz \Big\}/i = \\ &\Big\{ -LK^*_{tip}u(L) - Kr^*_{tip}\frac{\partial u}{\partial z}\Big|_L - m - Kr^*_{top}\frac{\partial u}{\partial z}\Big|_0 - \int_0^L zk_s(z)u(z)dz + \rho A\omega^2 \int_0^L zu(z)dz \Big\}/i, \end{aligned} \tag{14}$$

Now, for the other 3 equations, the same integrals are taken, but with variable integration bounds, focusing on a local part of the pile. The third integral is similar to equation 12 with bounds that are 'swept' with a stepsize ΔL focusing on the top of the pile. Hence, the lower integration bound $z^{(1)}_{f,t}$ ('f' for 'force', 't' for top and '$^{(1)}$' for lower integration bound) will start at the top of the pile ($z = 0$) and the upper will sweep until just above the tip. So,

$$\begin{aligned} z^{(1)}_{f,t} &= 0 \;..\; \Delta L \;..\; (L - 2\Delta L), \\ z^{(2)}_{f,t} &= z^{(1)}_{f,t} + \Delta L \;..\; \Delta L \;..\; L - \Delta L, \end{aligned} \tag{15}$$

Similarly, a local integral of the moment (like equation 14) is computed for the top of the pile, and the 5th integral is also an integral of the moment, but than including the tip of the pile, and not the top. With the 2 global and these 3 local integrals, we have 5 integrals that give a linear set of equations in $p_0..p_4$ (equation 11) and a resulting $c(z)$ for every combination of the integration bounds. All combinations of the 6 integration bounds are evaluated. Every found $c(z)$ is verified to be positive definite, and if so, the corresponding complex deflection and rotation are calculated according to equations 6 to 10, including the previously found complex discrete springs and $k_s(z)$. For the found deflection and rotations of the 1D model, the quality of the fit is assessed by considering the cost of the fit as

$$Cost_{u+u'} = Cost_u + Cost_{u'} = \frac{\sum_{i=0}^{i=L} |u_{3D,i} - u_{1D,i}|}{2\sum_{i=0}^{i=L} |u_{3D,i}|} + \frac{\sum_{i=0}^{i=L} |u'_{3D,i} - u'_{1D,i}|}{2\sum_{i=0}^{i=L} |u'_{3D,i}|}. \tag{16}$$

This cost is calculated for both the imaginary as the real parts of the deflection and rotation separately.

When following this procedure for finding the static stiffness, $k_s(z)$, we get the 'best' stiffness profile as given by Figure 6. The stiffness profiles given in Figure 6 results in a fit of the displacement u and the rotation (the first derivative of the displacement with respect to z) u' as given in Figure 5. This solution was found by sweeping the integration bounds with a stepsize of $\Delta L = 1.92m$.

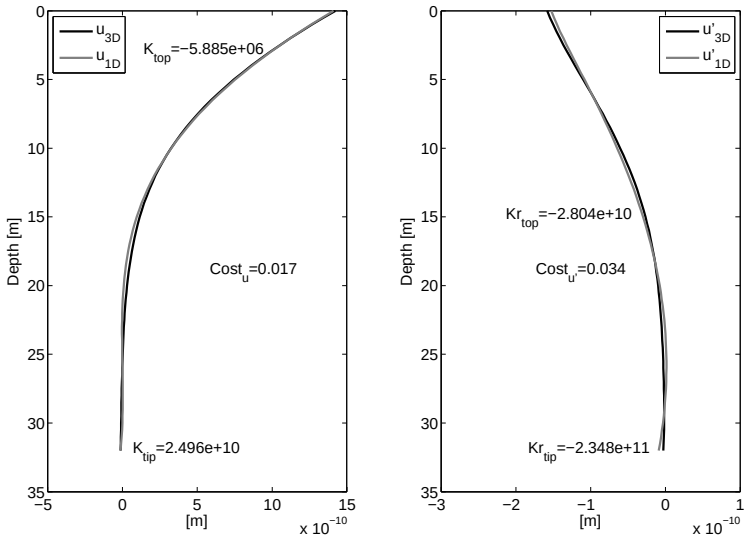

Figure 5: Static deflection u (left panel) and rotation u' (right panel): comparison of the 3D and the equivalent 1D model.

Continuing the above described procedure for the dynamic deflection, resulting from exciting the 3D pile with a unit lateral force (1N, no moment) at a frequency of 0.2 Hz, the $c(z)$ that gives the best solution when sweeping the integral bounds with a stepsize of $\Delta L = 2.13m$, is given in Figure 6. This Figure also includes $k_s(z)$ to be able to compare. Please note that the values of $k_s(z)$ are an order 100 larger than c(z), and that the unit is different.

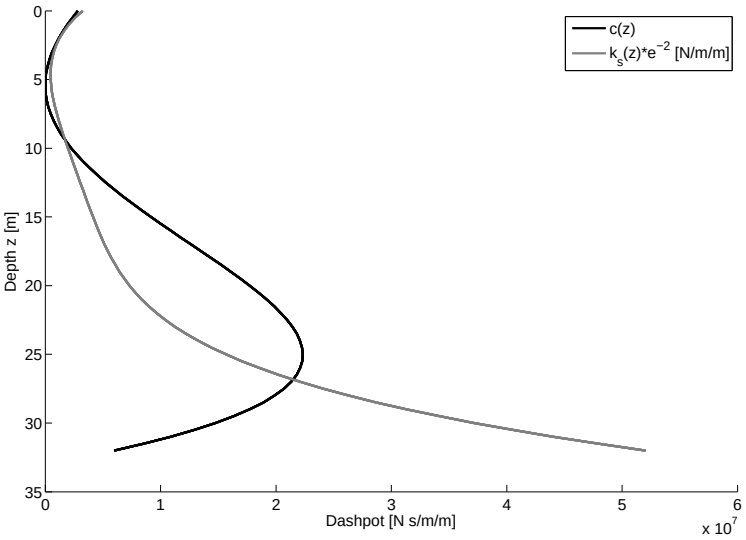

Figure 6: Resulting $k_s(z)$ from the static comparison of the models, and the 'best' c(z) for the case of a dynamic excitation of 0.2 Hz.

The corresponding fit between the imaginary parts of the 3D and 1D complex deflection is given in Figure 7, and the fit of the real parts of the complex rotations are given in Figure 8.

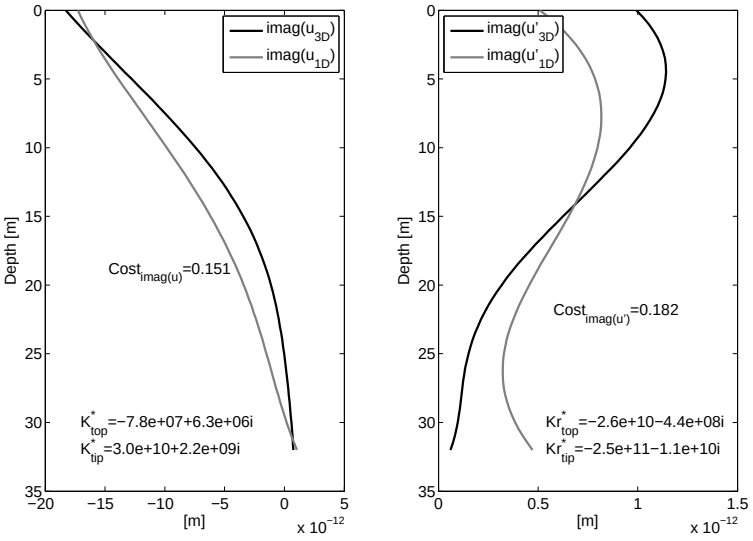

Figure 7: Comparison of the imaginary parts of the deflection (left panel) and rotation (right panel) of the 3D and the equivalent 1D model.

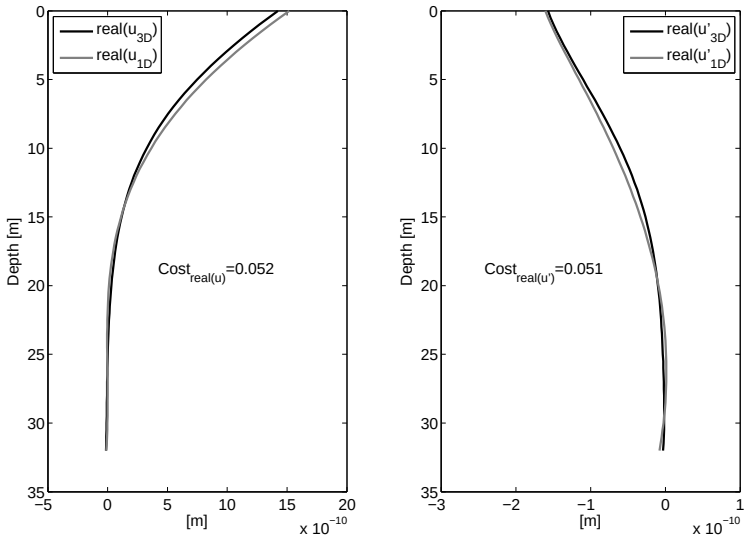

Figure 8: Comparison of the real parts of the deflection (left panel) and rotation (right panel) of the 3D and the equivalent 1D model.

5 Discussion & Conclusions

From the presented Figures (5 to 8) we see that a reasonable correspondence is found between the static deflection and rotation of the 1D and 3D model in case a unit horizontal force is applied at the top of the pile. The cost of the fit of the static displacement over the full length of the pile is 0.017, which can be multiplied by 2 to yield the percentage difference (see equation 16); 3.4%. The static rotations show a 6.8% difference. Similar matching efforts performed by Varun et al. [8], yielded a difference in static displacement at the top of the pile of 14.0%, and a difference in rotation at the same location of 8.7%. If we also only consider the top of the pile, the match in static deflection at this location is within 1% and the rotation is fitted within 3.4% accuracy.

When the pile is harmonically excited at 0.2 Hz with the same unit horizontal force amplitude, the real part of the complex response matches that of the 3D model with an overall 10.3% difference (10.4% for the displacement and 10.2% for the rotation over the full length of the pile). However, the fit of the imaginary parts of both the deflection and the rotation leave enough room for improvement; 30.2% and 36.4% difference in overall displacement and rotations respectively.

The cause of the discrepancy between the imaginary parts of the complex response will be investigated. One of the reasons could be that we assume that the static soil stiffness $k_s(z)$ (found in the first step where the static models are matched) also applies for the dynamic case. Possibly, this stiffness needs to be updated for the dynamic loading case.

Another aspect of the presented results that raises questions, is the fact that in

order for the edges of the 3D pile to match the classic Euler-Bernoulli conditions at the boundaries, negative rotational springs are needed to meet the balance of bending moment (equations 8 and 10). This contradicts our rule of not allowing negative stiffness in the 1D model. The fact that the soil reaction indeed causes a bending moment at the tip of the pile (and also distributed over its length) might not be too surprising. However, the need of the discrete 'balancing' springs at the top of the pile where the load is applied, indicates that discrepancies exist between the 3D pile mechanisms, and the Euler-Bernoulli theory.

References

[1] H.G. Poulos, Behavior of Laterally Loaded Piles I. Single Piles, Journal of Soil Mechanics & Foundations Div, 97.5, Proc paper 8092, 711-731, 1971

[2] B.M. Das, Principles of Foundation Engineering, 5th Edition, 2nd reprint, 2004

[3] P. Cuéllar, et al., A numerical model for the transient analysis of offshore foundations under cyclic loading, Computers and Geotechnics, 59, 75-86, 2014

[4] P.L.C. van der Valk, Coupled Simulations of Wind Turbines and Offshore Support Structures: Strategies based on the Dynamic Substructuring Paradigm, PhD Thesis, Delft University of Technology, 2014

[5] W.G. Versteijlen, et al., Assessing the small-strain soil stiffness for offshore wind turbines based on in situ seismic measurements, Journal of Physics: Conference Series 524.1, p. 012088, IOP Publishing, 2014

[6] O.C. Zienkiewicz and R.L. Taylor, The finite element method for solid and structural mechanics. Elsevier Butterworth-heinemann, 6th edition, 2005.

[7] E. Kausel and J.M. Oliveira Barbosa, PMLs: A direct approach, International Journal for Numerical Methods in Engineering 90.3, 2012, 343-352

[8] Varun, et al., A simplified model for lateral response of large diameter caisson foundationslinear elastic formulation, Soil Dynamics and Earthquake Engineering 29.2, 268-291, 2009

W.G. Versteijlen, Siemens Wind Power, Beatrixlaan 800, 2595 BN Den Haag, The Netherlands

A.V. Metrikine & K.N. van Dalen, Faculty of Civil Engineering and Geosciences, Delft University of Technology, Stevinweg 1, 2628CN Delft, The Netherlands